

# **NAVAL POSTGRADUATE SCHOOL**

## **Monterey, California**



## **THESIS**

**PERFORMANCE MEASUREMENT OF A MINI  
THERMOACOUSTIC REFRIGERATOR AND  
ASSOCIATED DRIVERS**

by

Denys Petrina

June 2002

Thesis Advisor:  
Second Reader:

Thomas J. Hofler  
Bruce Denardo

**Approved for public release; distribution is unlimited**

THIS PAGE INTENTIONALLY LEFT BLANK

<b>REPORT DOCUMENTATION PAGE</b>			Form Approved OMB No. 0704-0188	
Public reporting burden for this collection of information is estimated to average 1 hour per response, including the time for reviewing instruction, searching existing data sources, gathering and maintaining the data needed, and completing and reviewing the collection of information. Send comments regarding this burden estimate or any other aspect of this collection of information, including suggestions for reducing this burden, to Washington headquarters Services, Directorate for Information Operations and Reports, 1215 Jefferson Davis Highway, Suite 1204, Arlington, VA 22202-4302, and to the Office of Management and Budget, Paperwork Reduction Project (0704-0188) Washington DC 20503.				
<b>1. AGENCY USE ONLY (Leave blank)</b>		<b>2. REPORT DATE</b> June 2002	<b>3. REPORT TYPE AND DATES COVERED</b> Master's Thesis	
<b>4. TITLE AND SUBTITLE:</b> Performance Measurement of a Mini Thermoacoustic Refrigerator and Associated Drivers			<b>5. FUNDING NUMBERS</b>	
<b>6. AUTHOR(S)</b> Denys Petrina				
<b>7. PERFORMING ORGANIZATION NAME(S) AND ADDRESS(ES)</b> Naval Postgraduate School Monterey, CA 93943-5000			<b>8. PERFORMING ORGANIZATION REPORT NUMBER</b>	
<b>9. SPONSORING /MONITORING AGENCY NAME(S) AND ADDRESS(ES)</b> N/A			<b>10. SPONSORING/MONITORING AGENCY REPORT NUMBER</b>	
<b>11. SUPPLEMENTARY NOTES</b> The views expressed in this thesis are those of the author and do not reflect the official policy or position of the Department of Defense or the U.S. Government.				
<b>12a. DISTRIBUTION / AVAILABILITY STATEMENT</b> Approved for public release; distribution is unlimited			<b>12b. DISTRIBUTION CODE</b>	
<b>13. ABSTRACT</b>  A miniature Thermoacoustic refrigerator is being developed to cool integrated circuits – which must sometimes operate at high temperatures nearing the upper threshold of their tolerance – to temperature spans more within the circuits' tolerable limits, without the need of the chemicals of a traditional refrigerating system. The development of an electrically powered acoustic driver that powers the thermoacoustic refrigerator is described, as well as different schemes to improve its delivered acoustic power. The driver utilizes a flexural tri-laminar piezoelectric disk to generate one to two Watts of acoustic power at 4 kHz in 15 bar of He-Kr gas mixture. Two different drivers are tested on a pressurized test resonator, and their quantitative performance is analyzed. The analysis of the drivers' performance indicates one power-improvement scheme may be faulty, while data taken before the second broke indicates its design may be beneficial to power-improvement. Tests are also conducted using a refrigerating resonator; these first attempts to meet design criteria of temperature span and cooling power are unsuccessful, but the results obtained – including a thermodynamic coefficient of performance (COP) 13.1% below the modeled ideal value for the given data set – with less-than-ideal acoustic power delivered to the resonator signal suggest continued research is worthwhile.				
<b>14. SUBJECT TERMS</b> Thermoacoustic refrigerator, TAR, thermo-acoustic refrigerator driver, microchip cooling			<b>15. NUMBER OF PAGES</b> 59	
			<b>16. PRICE CODE</b>	
<b>17. SECURITY CLASSIFICATION OF REPORT</b> Unclassified	<b>18. SECURITY CLASSIFICATION OF THIS PAGE</b> Unclassified	<b>19. SECURITY CLASSIFICATION OF ABSTRACT</b> Unclassified	<b>20. LIMITATION OF ABSTRACT</b> UL	

THIS PAGE INTENTIONALLY LEFT BLANK

**Approved for public release; distribution is unlimited**

**PERFORMANCE MEASUREMENT OF A MINI THERMOACOUSTIC  
REFRIGERATOR AND ASSOCIATED DRIVERS**

Denys E. Petrina  
Ensign, United States Navy  
B.S., Rensselaer Polytechnic Institute, 2001

Submitted in partial fulfillment of the  
requirements for the degree of

**MASTER OF SCIENCE IN  
APPLIED PHYSICS**

from the

**NAVAL POSTGRADUATE SCHOOL  
June 2002**

Author: Denys Petrina

Approved by: Thomas J. Hofler  
Thesis Advisor

Bruce Denardo  
Second Reader/Co-Advisor

William B. Maier II  
Chairman, Department of Physics

THIS PAGE INTENTIONALLY LEFT BLANK

## ABSTRACT

A miniature Thermoacoustic refrigerator is being developed to cool integrated circuits – which must sometimes operate at high temperatures nearing the upper threshold of their tolerance – to temperature spans more within the circuits' tolerable limits, without the need of the chemicals of a traditional refrigerating system. The development of an electrically powered acoustic driver that powers the thermoacoustic refrigerator is described, as well as different schemes to improve its delivered acoustic power. The driver utilizes a flexural tri-laminar piezoelectric disk to generate one to two Watts of acoustic power at 4 kHz in 15 bar of He-Kr gas mixture. Two different drivers are tested on a pressurized test resonator, and their quantitative performance is analyzed. The analysis of the drivers' performance indicates one power-improvement scheme may be faulty, while data taken before the second broke indicates its design may be beneficial to power-improvement. Tests are also conducted using a refrigerating resonator; these first attempts to meet design criteria of temperature span and cooling power are unsuccessful, but the results obtained – including a thermodynamic coefficient of performance (COP) 13.1% below the modeled ideal value for the given data set – with less-than-ideal acoustic power delivered to the resonator signal suggest continued research is worthwhile.

THIS PAGE INTENTIONALLY LEFT BLANK



## TABLE OF CONTENTS

<b>I.</b>	<b>INTRODUCTION .....</b>	<b>1</b>
<b>A.</b>	<b>OBJECTIVE .....</b>	<b>1</b>
<b>B.</b>	<b>THESIS ORGANIZATION .....</b>	<b>2</b>
<b>II.</b>	<b>BACKGROUND .....</b>	<b>3</b>
<b>A.</b>	<b>HEAT ENGINES .....</b>	<b>3</b>
<b>B.</b>	<b>THERMOACOUSTIC HEAT ENGINES .....</b>	<b>5</b>
<b>C.</b>	<b>DELTA-E AND DSTAR COMPUTER MODELS .....</b>	<b>7</b>
<b>III.</b>	<b>HISTORY.....</b>	<b>9</b>
<b>A.</b>	<b>BROOKS DEMO-TAR .....</b>	<b>9</b>
<b>B.</b>	<b>MINI-TAR.....</b>	<b>10</b>
<b>IV.</b>	<b>DESIGN OF THE MINI-TAR DRIVER .....</b>	<b>13</b>
<b>A.</b>	<b>FRONT PLATE .....</b>	<b>13</b>
<b>B.</b>	<b>BACK PLATE .....</b>	<b>16</b>
<b>C.</b>	<b>DRIVER BODY .....</b>	<b>17</b>
<b>V.</b>	<b>EXPERIMENTAL SET-UP .....</b>	<b>19</b>
<b>A.</b>	<b>TEST RESONATOR.....</b>	<b>19</b>
<b>B.</b>	<b>MEASUREMENT SET-UP .....</b>	<b>20</b>
<b>VI.</b>	<b>DRIVER ENHANCEMENT.....</b>	<b>23</b>
<b>A.</b>	<b>SCHEMES .....</b>	<b>23</b>
<b>1.</b>	<b>Diaphragm Size .....</b>	<b>23</b>
<b>2.</b>	<b>Mass Weighting .....</b>	<b>23</b>
<b>3.</b>	<b>Number of Discs .....</b>	<b>24</b>
<b>4.</b>	<b>Diaphragm Pre-flexing .....</b>	<b>24</b>
<b>B.</b>	<b>PAST WORK .....</b>	<b>25</b>
<b>1.</b>	<b>SN-01.....</b>	<b>25</b>
<b>2.</b>	<b>SN-02.....</b>	<b>25</b>
<b>VII.</b>	<b>MEASUREMENTS .....</b>	<b>27</b>
<b>A.</b>	<b>DRIVER SN-03 .....</b>	<b>27</b>
<b>1.</b>	<b>Gas Resonance .....</b>	<b>27</b>
<b>2.</b>	<b>Refrigeration Tests .....</b>	<b>29</b>
<b>B.</b>	<b>SN-04.....</b>	<b>31</b>
<b>C.</b>	<b>SN-05.....</b>	<b>33</b>
<b>VIII.</b>	<b>ANALYSIS OF REFRIGERATION DATA.....</b>	<b>35</b>
<b>A.</b>	<b>THERMAL IMPEDANCE .....</b>	<b>35</b>
<b>B.</b>	<b>REFRIGERATOR UNDER LOAD .....</b>	<b>35</b>
<b>IX.</b>	<b>CONCLUSIONS .....</b>	<b>39</b>
<b>A.</b>	<b>DRIVER-POWER IMPROVEMENT SCHEMES .....</b>	<b>39</b>

B.	MINI-TAR REFRIGERATION.....	39
C.	RECOMMENDATIONS OF FUTURE WORK .....	40
D.	OVERALL.....	40
LIST OF REFERENCES .....		41
INITIAL DISTRIBUTION LIST.....		43

## LIST OF FIGURES

Figure 2.2.	Simple Thermoacoustic Engine (From: Purdy, 1998, pg. 9).....	6
Figure 3.1.	Brooks DemoTAR. The white is frost formed on the cold heat exchanger. ..	10
Figure 4.1.	CAD Drawing of Front Plate. ....	14
Figure 4.2.	Side view of top plate. Note the three piezoelectric discs in the center, and microphone to left of discs. ....	15
Figure 4.3.	Capillary tube cavity schematic. ....	15
Figure 4.4.	Top of the front plate. The white is the Teflon gasket; the innermost circle is the screw that holds the pushrod to the diaphragm (shadowed). ....	16
Figure 5.1.	The Test resonator, shown with a single-disc driver. ....	20
Figure 5.2.	Overview of the measurement setup.....	21
Figure 6.1.	Mass-weighting of a two-disc driver. ....	24
Figure 7.1.	Resonance plot of 18% Ar-He. The peaks at 3.17 kHz denote the gas resonance, while the peaks on the right show the driver resonance. ....	28
Figure 7.2.	Individual gas resonances. The plots are not continuous over the entire range of frequencies as the frequency sweeps of interest were not in the same range. ....	29
Figure 7.3.	Location of the thermocouple on the cold heat exchanger with the leads at top-right, and the resistor on the cold heat exchanger with leads at top-left. ..	30

THIS PAGE INTENTIONALLY LEFT BLANK

## LIST OF TABLES

Table 7.1.	Heat Leak Measurement Data. ....	31
Table 7.2.	Temperatures vs. Heat Load. ....	31
Table 7.3.	Resonance peaks for SN-04 at different pressures. ....	32
Table 8.2.	Determining total heat load on the MiniTAR. ....	36
Table 8.3.	Actual Figures-of-Merit vs. Theoretical. ....	37

THIS PAGE INTENTIONALLY LEFT BLANK

## **ACKNOWLEDGMENTS**

I would like to thank Dr. Hofler for the many hours spent explaining, and then re-explaining, whatever I couldn't get into my head.

Thanks also to Dr. Denardo for being a Co-Advisor and reviewing the second draft of this thesis.

THIS PAGE INTENTIONALLY LEFT BLANK



# **I. INTRODUCTION**

Thermoacoustic refrigeration uses advanced acoustic technology to improve cooling capacity without the need for environmentally destructive refrigerants. The subject of Dr. Thomas Hofler's doctoral research, the thermoacoustic refrigerator (TAR) is a test-bed for thermoacoustic theory and a major step toward achieving a practical thermoacoustic cryocooler.

The mechanism of the TAR is simple, based on the expansion and compression of a gas by a sound wave. When a sound wave from a vibrating diaphragm or loudspeaker is sent down a half-wavelength tube, the pressure pulsations form a standing wave, which causes oscillatory motion of the gas in the tube's axial direction.

The combination of pressure oscillation and oscillatory motion of the gas causes heat transport wherever the gas is in thermal contact with a stationary surface. If a small structure with a large amount of surface area is placed in an appropriate location in an intense standing wave, substantial amounts of heat transport will occur, with one end cooled by the heat transport, and the other end heated. This structure is usually called a "stack"; if both ends of the stack make thermal contact with heat exchangers, a functional heat pump or refrigerator can be constructed.

## **A. OBJECTIVE**

The objective of this thesis project is two-fold: to evaluate the performance of different drivers designed for a mini thermoacoustic refrigerator (MiniTAR), and to conduct initial refrigeration tests of the MiniTAR.

The MiniTAR is designed to cool micro-electronic integrated circuits in order to prevent malfunction in very warm ambient conditions. Constructed of a custom piezoelectric driver and a copper & stainless-steel resonator, it is intended to match the levels of efficiency and durability set by existing thermoelectric coolers. Future versions are intended to surpass these levels.

## **B. THESIS ORGANIZATION**

Chapter II offers a review of some basic thermodynamics, and then applies those principles to acoustics, providing a simple foundation for the following chapters.

Chapter III discusses a previous, successful TAR, and how that TAR's design was applied to the MiniTAR.

Chapter IV discusses the specific design of the MiniTAR driver.

Chapter V explains the laboratory set-up used to collect data. Also explained is any custom apparatus used to collect these measurements.

Chapter VI gives an explanation of the different schemes proposed to improve driver power. Past work on this specific subject is also reviewed.

Chapter VII recounts actual testing, presents all data collected, and analyzes driver-only measurements.

Chapter VIII is specifically dedicated to analyzing the measurements taken in the first MiniTAR refrigeration tests.

In concluding this thesis, Chapter IX offers general observations and makes recommendations for further work.

## II. BACKGROUND

### A. HEAT ENGINES

Thermodynamics is, of itself, the study of temperature and the transfer of thermal energy, the transfer usually being between a "hot" reservoir at temperature  $T_H$  and a "cold" reservoir at temperature  $T_C$ , with  $T_H > T_C$ . If a machine performs a transfer of thermal energy, with useful purpose, it is called a "heat engine". The MiniTAR is classified as a Thermoacoustic Heat Engine. Heat engines are further classified according to what is done with heat; refrigerators and "heat pumps" require Work to transfer heat from cold to hot, while "prime movers" output Work in a transfer of heat from hot to cold.

The First Law of Thermodynamics states that for any thermodynamic process, the total energy of the system must be conserved. For expressing this fact in an equation, let  $Q_H$  and  $Q_C$  be the amount of heat transferred to (or from) the hot and cold reservoir, respectively, and  $W$  the Work; therefore:

$$Q_H - Q_C = W$$

The Second Law of Thermodynamics states that a perfect refrigerator working in a cycle must utilize physical processes in the transfer of heat from cold to hot, and said processes must be 100% reversible – consequently, a perfect refrigerator requires Work input and  $Q_H > Q_C$ . Conversely, the Second Law states that a perfect prime mover working in a cycle must utilize reversible physical processes when extracting heat from the hot reservoir and cannot produce an equivalent amount of Work – consequently, some heat is transferred to the cold reservoir and  $Q_H > W$ . Fig 2.1 graphically shows the basic operation of the two types of heat engine.

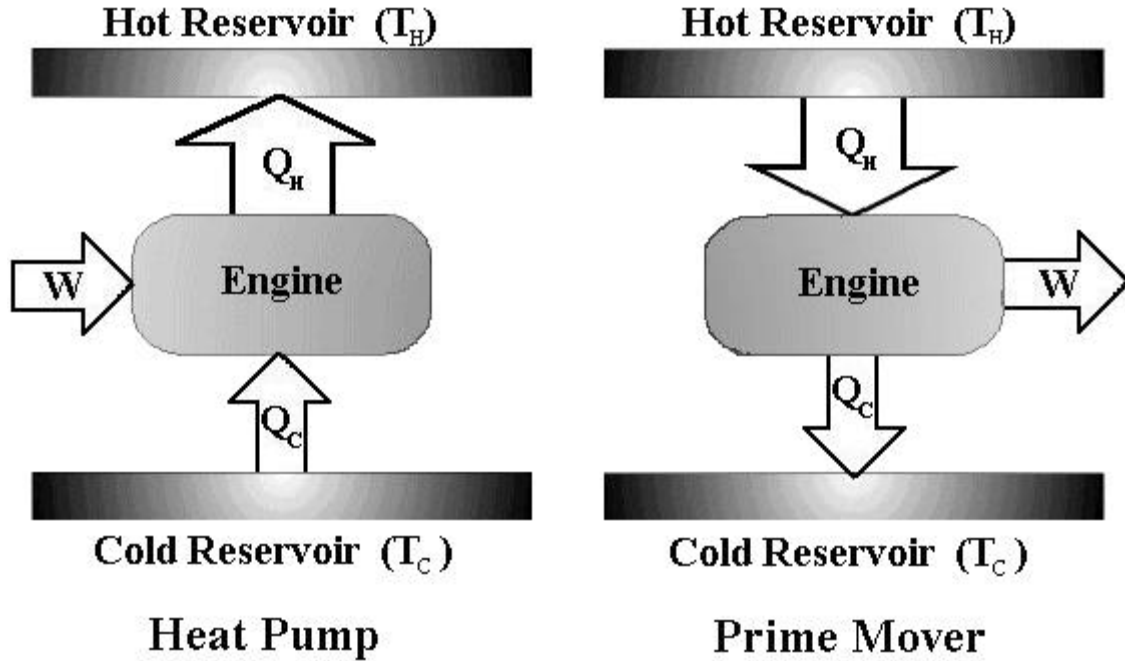


Figure 2.1. Heat Engine Operation (From: Livvarcin, 2000, pg. 9)

The figure-of-merit or “efficiency”  $\epsilon$  of a prime mover is defined as the ratio of the work done to the heat absorbed, i.e.:

$$\epsilon = \frac{W}{Q_H} = 1 - \frac{|Q_C|}{Q_H}$$

Coupled with the Second Law of Thermodynamics, it is impossible to have a heat engine with  $\epsilon=1$ ; there is, however, a maximum *possible* efficiency.

Carnot theorized that no heat engine working in one direction between two reservoirs can have a greater efficiency than a reversible engine operating between the same two reservoirs. The quantitative efficiency of a reversible or “perfect” heat engine can also be obtained directly from the Second Law, which historically came later. The *Carnot efficiency*  $\epsilon_C$  is defined as:

$$\epsilon_C = 1 - \frac{T_C}{T_H}.$$

In the case of an engine operating as a heat pump, a more useful and common figure-of-merit is the *coefficient of performance* (COP) given by:

$$COP = \frac{Q_C}{W}$$

where  $W$  is the energy input required by the engine to achieve the desired effect  $Q_C$ . Using  $Q_C = Q_H - W$  and the reciprocal of  $\epsilon_C$  to eliminate  $Q_H$ , we reach:

$$COP = \frac{T_C}{T_H - T_C}$$

## B. THERMOACOUSTIC HEAT ENGINES

A Thermoacoustic Heat Engine makes use of basic gas properties: assuming a constant molar amount of gas in a container, the gas will increase in temperature when compressed, and decrease in temperature when allowed to expand. In thermoacoustics, the compression of the gas is made possible by an acoustic wave, which is itself a pressure wave.

A TAR is made of two individual assemblies: 1) the driver, and 2) the resonator. The input Work required for refrigeration is converted from whichever input form (for a MiniTAR, electricity) into acoustic waves in the driver. The actual refrigeration occurs in the resonator, discussed here.

The resonator assembly contains four basic components needed for refrigeration: 1) the hot heat exchanger, which is the interface for the reservoir at temperature  $T_H$ ; 2) the cold heat exchanger (interface for  $T_C$ ); 3) the resonator tube; and 4) the acoustic stack. Figure 2.3 shows the physical arrangement of these parts within the resonator, as well as their relation to the driver.

## Simple Thermoacoustic Heat Engine

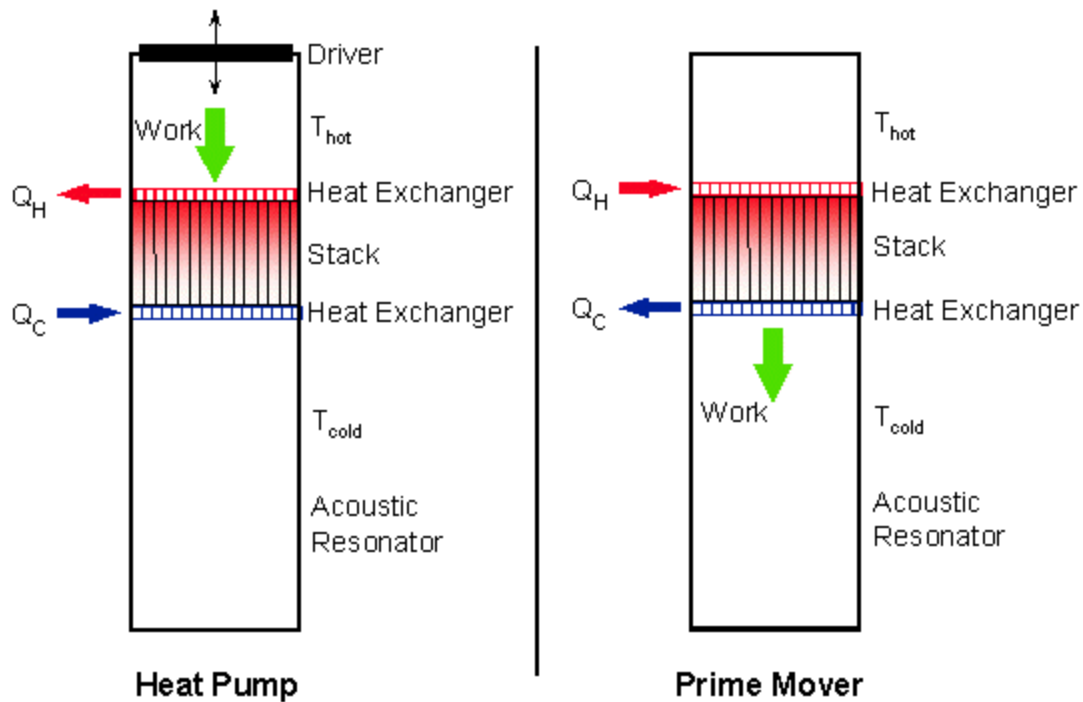


Figure 2.2. Simple Thermoacoustic Engine (From: Purdy, 1998, pg. 9)

During the design phase, the driver and resonator tube are matched so the tube is one-quarter wavelength long; this allows a standing wave to form in the tube, with a resonance quality factor in the range of 10 to 30. The stack is placed inside the tube very near a pressure antinode of the standing wave – typically a distance of 1/50 of a wavelength.

The stack itself is commonly a multilayered (rolled) combination of polyester plastic film and monofilament line used as spacer between layers. The layers create channels through which the acoustic wave travels. They are parallel to the direction of wave propagation and serve as a conduit for the transfer of heat and acoustic power. The interaction between the oscillating gas (in the channels of the stack) and the stack surface causes heat to be transported from one end of the stack to the other, towards the pressure antinode.

The size of a single channel cross-section is typically two to four thermal penetration depths,  $\delta_\kappa = \sqrt{\frac{2\chi}{\omega}}$ , where  $\delta_\kappa$  is the approximate distance heat can diffuse in one acoustic cycle,  $\chi$  the thermal diffusivity of the gas, and  $\omega$  the radial frequency. The compression and expansion of the gas in the channel is neither isothermal nor adiabatic, therefore, temperature oscillations exist and heat diffuses transversely between the gas and adjacent solid surface area. The spacing of a few  $\delta_\kappa$  leads to temperature oscillations in the gas that are not in phase with the acoustic pressure oscillations. This phase difference between pressure and temperature leads to a non-zero time-averaged heat flow along the stack surface.

Looking again at Fig. 2.2, the lowest resonant mode is a quarter wavelength with pressure anti-nodes at the closed end and pressure nodes at the open end. This configuration ensures that the fundamental will have a wavelength approximately four times the length of the tube. Other configurations are possible, including a closed end resonator with pressure antinodes at both ends producing acoustic power at a wavelength two times the physical length of the tube.

As applied to the MiniTAR, the stack is placed within the tube so the hot heat exchanger is located closest to the pressure antinode; as heat flows toward the antinode, "cold" is left at the other end of the stack, which can be used for refrigeration if a cold heat exchanger is located at this point.

Another factor taken into the design of the resonator is the pressure differential caused by the acoustic wave ( $p_o$ ) compared to the mean pressure of the resonator ( $p_m$ ). All TARs designed at the Naval Postgraduate School are designed to best operate when the ratio of pressure differential to mean pressure is  $\frac{p_o}{p_m} = 5\%$ .

### C. DELTA-E AND DSTAR COMPUTER MODELS

The above discussion only covers the most basic of the physical concepts involved in Thermoacoustic Refrigeration; other factors of design include desired cooling output, desired gas mixture, temperature range of operation, and etc. To factor in

all of these considerations, two computer modeling programs have been developed: DeltaE at Los Alamos National Laboratory, and DSTAR at the Naval Postgraduate School.

DeltaE is the more full-featured of the two systems – it has been near-constantly refined due to the various Thermoacoustic projects undertaken at Los Alamos, and in so doing covers almost any imaginable thermoacoustic engine component.

DSTAR (Design and Simulation for Thermoacoustic Refrigerators) is a C++-based program developed under the direction of Dr. Thomas J. Hofler as a user-friendly and in-house alternative to the command-line DeltaE. DSTAR also offers an ability to work with different units, or in dimensionless units if desired. The dimensionless units feature greatly facilitates the design phase of a project, while the option of English or metric units allows the direct comparison of experimental measurements to theoretical output. The main drawback of the program is its limited set of engine components.



### III. HISTORY

#### A. BROOKS DEMO-TAR

To date, the MiniTAR is the latest of six different TARs to be built under Professor Hofler's supervision. Of the previous five, the Brooks DemoTAR is one of the more successful designs and is the most consistent with the performance requirements set for the MiniTAR. Its design was therefore the starting point in designing the MiniTAR.

The Brooks DemoTAR was designed and initially constructed by LT Brent Brooks (US Navy), with construction completed and testing done by LT Todd Berhow (US Navy). The DemoTAR was conceived in 1994 after the somewhat lackluster reception of an earlier demonstration refrigerator built for a meeting of the Acoustical Society of America; the cold end temperature reached 8.9 °C, and could only be observed on a thermometer via a thermocouple – there were no other visual cues of the refrigerator's cooling power.

To give a more impressive demonstration, it was desired that the new DemoTAR, during the course of a short lecture in a crowded room, produce frost that could be readily seen and touched. To produce frost, the unit was designed to reach a cold heat exchanger temperature of  $T_C = -5$  °C, while expelling heat to the room at  $T_H = 25$  °C. This external  $\Delta T_E = 30$  K does not reflect any temperature differences that may occur due to heating of the internal heat exchangers and heat exchange with the room air – for this, an additional 10 K was added to arrive at internal  $\Delta T_I = 40$  K. Thus, during the design phase, the "desired" cold heat exchanger temperature effectively became  $T_C = -15$  °C; the temperature differences could therefore "bump-up" the cold temperature to  $T_C = -5$  °C without incurring an unplanned loss. For a Thermoacoustic heat engine (as well as a Carnot cycle engine) the important temperature parameter is given by the ratio:

$$\frac{T_H}{T_C} = \frac{298K}{258K} = 1.16$$

During the design phase, the resonator's parameters were optimized to a driver producing 10 W of power at 650 Hz and the vessel pressurized with helium to 90 psia.

As part of his thesis, Brooks, using C-code written by Professor Hofler, optimized the stack's length and position in the resonator tube, as well as the stack layer spacing. A notable result was the ability to cut the length of the resonator tube by 40% relative to an optimum efficiency resonator – when coupled with a slight decrease of the tube's diameter, predicted cooling losses from shortening the tube were deemed allowable. Numbers in hand, Brooks predicted that at  $p_o/p_m = 5\%$ , total cooling power would be 11.1 Watts, with a temperature span = 35 °C, COP = 1.15, and efficiency  $\varepsilon = 0.15$ .

In testing, Berhow determined that at  $p_o/p_m = 5\%$  and under a heat load, total cooling power was 10.82 watts, with a temperature span = 32.4 °C, COP = 1.00, and  $\varepsilon = 0.121$ . See Fig. 3.1.



Figure 3.1. Brooks DemoTAR. The white is frost formed on the cold heat exchanger.

## B. MINI-TAR

In the year 2000, Rockwell Science Center (RSC) contracted to the Naval Postgraduate School a project to design and construct a MiniTAR. RSC's original desired specifications for the MiniTAR was to produce 1 W of cooling power between 60 °C and 90 °C ( $\Delta T_E = 30$  K) when operating at 10 kHz, all in a package that was 1 inch in total length. Later on, due to difficulties in designing such small components and in finding a driver that would operate at 10 kHz, the performance expectations were

modified: the operating frequency was lowered to 4 kHz, and the allowable length was increased to 2 inches.

During design, 6° K of internal cooling were thought required, so  $\Delta T_I = 36K$ . Thus, the ratio  $T_H:T_C$  for the MiniTAR:

$$\frac{T_H}{T_C} = \frac{363K}{327K} = 1.11$$

which is similar but lower than the same ratio for the DemoTAR. Coupled with the success of the DemoTAR, it was decided the MiniTAR resonator would be similar to a scaled-down version of the DemoTAR's resonator which was subsequently re-optimized with DSTAR. The next step was to design, build, and test a suitable piezoelectric driver.

THIS PAGE INTENTIONALLY LEFT BLANK

## IV. DESIGN OF THE MINI-TAR DRIVER

Aside from the initial refrigeration measurements with the pressurized Refrigerating resonator, the research for this thesis involved the testing and evaluation of various schemes considered to improve MiniTAR-driver performance. To gain a better appreciation of how these schemes will work, this chapter will cover the basic driver model, designed by Professor Hofler. The driver consists of three parts: the front plate assembly, the back plate, and the body.

### A. FRONT PLATE

A CAD drawing of the front plate is shown in Fig. 4.1. The reader is highly encouraged to view the drawing when reading the text.

Working from the edges inward, the outer ring of holes are drilled straight through the plate and are used to attach the front plate to the driver body with screws. The inner ring of screw holes do not go entirely through the plate (seen in Section B-B') – it is with these holes the driver is connected to the resonator.

The horizontal (white) bar seen in Sections A-A' and B-B' is the stainless-steel-foil diaphragm. A hole is drilled in the middle of the diaphragm, and the hollow aluminum pushrod is attached to the diaphragm using a stainless-steel screw. The piezo-electric disk(s) are then attached to the pushrod using epoxy EC2850FT, an electrically insulating adhesive. During MiniTAR operation, the disk(s) oscillate, which also cause the diaphragm to oscillate; the diaphragm oscillation, in turn, is the direct source of the acoustic (pressure) waves in the resonator. If the plate is held horizontally, the diaphragm/disk arrangement appears as in Fig. 4.2.

An additional two holes are drilled in the top plate: a microphone pass-through, and the capillary tube. The microphone is a pressure-sensitive DC microphone, used to measure pressure differential inside the resonator. The microphone appears as the small diameter vertical stainless-steel tube with a white TFE pressure seal collar in the left foreground of Fig 4.2.

Mini Driver Top  
Make 5 of 6061-T6 Aluminum

Notes: X.XXX tolerance is  $\pm 0.003$ "; X.X° tolerance is  $\pm 0.05^\circ$ .

Tom Hofler  
Physics  
Room SP-142  
X-2420  
tjhofler@nps.navy.mil

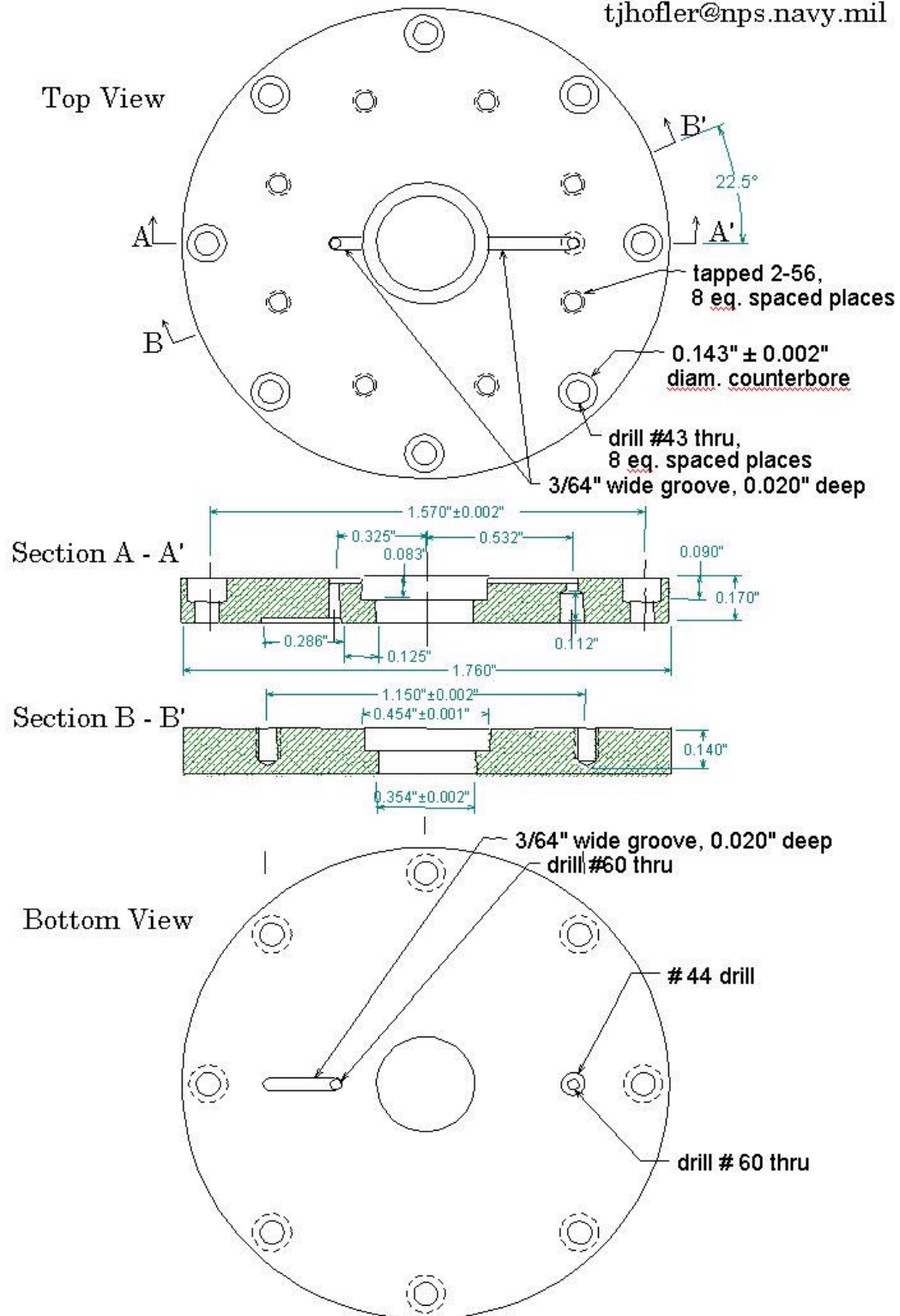


Figure 4.1. CAD Drawing of Front Plate.

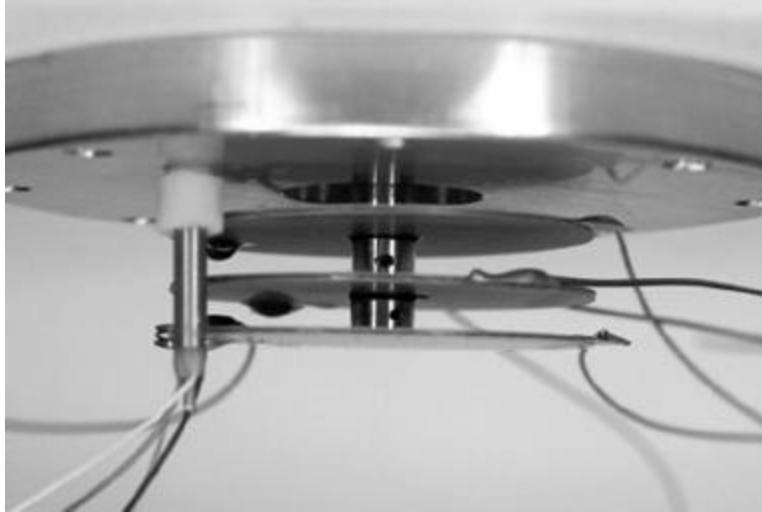


Figure 4.2. Side view of top plate. Note the three piezoelectric discs in the center, and microphone to left of discs.

The capillary tube provides for gas transfer between the driver and resonator. For the MiniTAR to optimally operate, both the driver and the resonator must be at the same static pressure. Taking into consideration the connection between the two is airtight, and a separate gas port for the resonator is undesirable, the diameter of the capillary tube is carefully chosen – if too large, it will reduce the dynamic acoustic pressure and power level; if too small, then there will be little pressure equalization and pressure differentials may then exceed levels that are safe for the diaphragm. A representation of the capillary tube cavity is shown in Fig 4.3. For more information about the installation and production of the capillary tube, see Livvarcin, 2000.

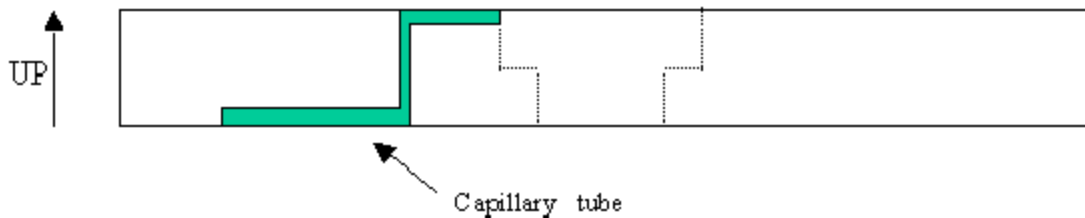


Figure 4.3. Capillary tube cavity schematic.

Finally, the metal-to-metal contact between driver and resonator will not prevent gas leakage. The solution to this problem is a Teflon gasket seal located around the

outside of the diaphragm, microphone hole, and capillary tube, but inside the resonator attachment screw holes. See Fig 4.4.

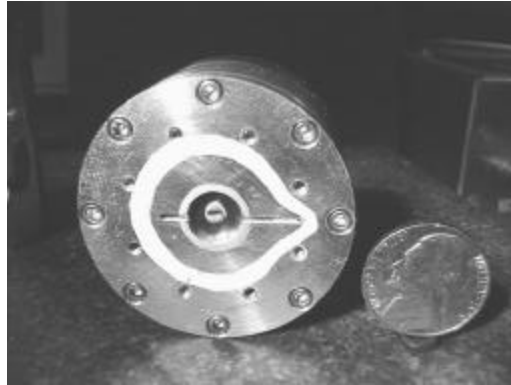


Figure 4.4. Top of the front plate. The white is the Teflon gasket; the innermost circle is the screw that holds the pushrod to the diaphragm (shadowed).

## **B. BACK PLATE**

There are four holes on the surface of the back plate. Two are for electrical feed-throughs of the power amplifier signal, another is a 4-pin electrical feed-through for the microphone, and the last a gas port for injecting the desired amount of gas into the MiniTAR.

Two gold-plated mini banana jacks are installed onto the back plate for the power amplifier connection. On the inside, two small pieces of wire are soldered to the legs of the jacks to provide a connection between banana jacks and the piezo disc(s). During installation, the jacks are first painted with 2850FT epoxy, then glued into the holes with the epoxy. The properties of the epoxy prevent gas leakage and provide electrical insulation from the metal plate.

The installation of the microphone is made complex by the microphone requiring four wires. If left insulated, the wires will cause significant gas leakage; bare wires, if allowed to touch, will create electrical shorts. During installation, the wires are held apart by use of a four-terminal connector and the epoxy. The microphone is included in the design for research purposes; a production model will not need a microphone and the complexities of its installation.



### **C. DRIVER BODY**

The driver's body is simply a hollow stainless-steel cylinder with open ends, two tapped machine screw hole circles, and two O-ring grooves for face seals. Its function is to create a sealed cavity between the front and back plates, wherein the piezoelectric components, microphone, and associated wiring reside.

THIS PAGE INTENTIONALLY LEFT BLANK

## **V. EXPERIMENTAL SET-UP**

Before proceeding, it is beneficial to first describe the methods of acquiring data when testing the individual drivers. This chapter will cover the Test resonator, system set-up, and basic measurement procedure.

### **A. TEST RESONATOR**

As previously stated, the main design challenge of the MiniTAR (other than its size) was finding a suitable driver. A concern was testing the proposed driver designs – for accurate measurements, the drivers had to be tested with an acoustic load approximating that of the Refrigerating resonator. For this, a separate Test resonator was built.

While the obvious method is to test the driver with the Refrigerating resonator, there are two reasons why a special Test resonator was built for the purpose of driver testing. First, the Test resonator could be built quickly and would allow driver testing to proceed without a lengthy wait for the completion of the Refrigerating resonator. Second, the Refrigerating resonator is actually a surprisingly poor test-bed for driver development; the high acoustic power levels required in driver testing are intimately connected to temperature changes and resultant resonant frequency changes in the Refrigerating resonator. The Test resonator was specifically designed for a high degree of temperature stability.

The Test resonator is effectively a simple copper-tube with a driver attachment point at one end and an adjustable plunger at the other, with an inner wall shaped to resemble an hourglass. See Fig. 5.1. This internal shape enables high amplitude standing waves without much distortion. The adjustable plunger allows for shifting the tube's resonant frequency. Optimally, the resonant frequency of the resonator must match the mechanical resonance of the driver, the latter not readily adjustable. When coupled with measurements from the SRS-785 Signal Analyzer (procedure described later in this chapter) and aided by theoretical calculations with DSTAR, the optimum operating frequency can be found and applied to resonator design.

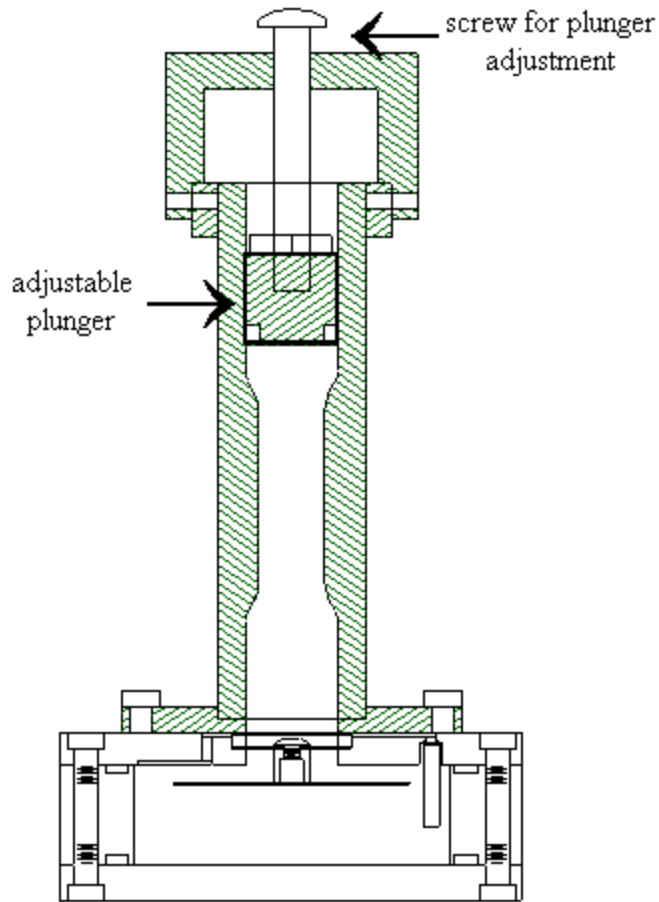


Figure 5.1. The Test resonator, shown with a single-disc driver.

Another note of the Test resonator's design: the Refrigerating resonator of the MiniTAR is designed to optimally operate at a pressure of 15 bar; designed with the aid of DSTAR, the Test resonator produces the equivalent acoustic load, but at 10 bar. More information on the Test resonator can be found in Direk, 2000.

## B. MEASUREMENT SET-UP

To take measurements, a SRS-785 two-channel signal analyzer, two multimeters, a preamplifier, a power amplifier, and a gas panel are arranged in a system, shown in Fig 5.2.

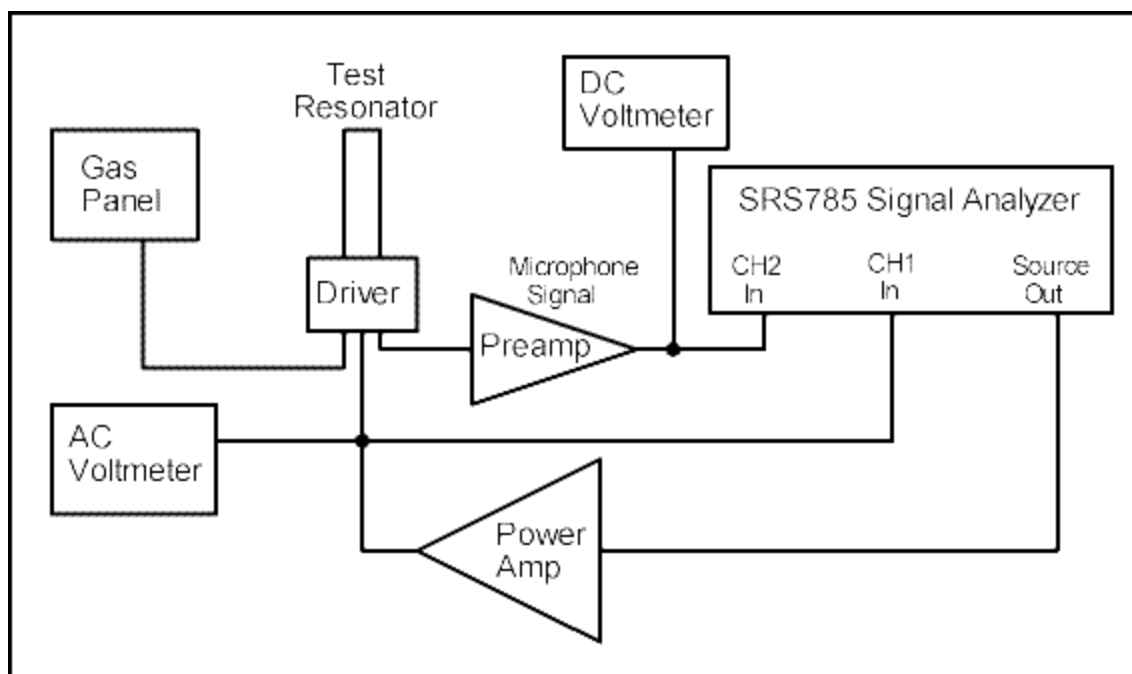


Figure 5.2. Overview of the measurement setup.

When a driver is mounted – either to the Test resonator or to the Refrigerating resonator – for measurements, the system is first purged. Purging consists of bleeding and using a vacuum pump to pump the assembly volume to 1 or 2 psia, repressurizing with the desired test-gas mixture (either helium, argon, or mixtures thereof) to 80 or 100 psia, and repeating the cycle three or four times. Once purging is complete, the gas panel is used to maintain near-constant pressure in the assembly, and measurements can now be taken.

For testing, the signal analyzer is operated in swept-sine mode to both generate signals to the driver and to record response. An input drive voltage is selected, and then the drive frequency is swept either up or down over a chosen range. All signals are first processed through a power amplifier, taking care to not exceed an imposed drive voltage limit of 15  $V_{\text{rms}}$  – damage begins to occur at 17  $V_{\text{rms}}$ . The power amplifier connects to the driver via miniature banana jacks, to the signal analyzer as a reference signal, and to a multimeter operating as an AC Voltmeter – this helps the operator ensure the 15  $V_{\text{rms}}$  limit is not exceeded.

Inside the assembly, the driver's microphone measures the absolute pressure amplitude developed inside the resonator. The microphone's signal is fed through a pre-amplifier to a multimeter – operating as a DC Voltmeter – and to the signal analyzer test signal input. The DC Volt read-out can be converted to pressure (explained in Chapter VII), and the signal analyzer is used for processing.

With the signal analyzer, the resonant frequencies of both driver and resonator can be seen in the frequency-response sweep, and with the Test resonator, hopefully matched by adjusting the plunger. Additionally, data collected by the signal analyzer can be saved to disk for later analysis.

## **VI. DRIVER ENHANCEMENT**

In designing the MiniTAR driver, four ideas were proposed to improve driver power – it was not known which idea(s) would be successful. This chapter will cover the various schemes proposed to improve performance, as well as past work leading-up to this thesis.

### **A. SCHEMES**

#### **1. Diaphragm Size**

"Diaphragm size" means the surface area of the diaphragm; it is theorized that of two drivers which vary only in the diaphragm size, the driver with larger diaphragm size will not only displace a large volume because of its increased surface, but also from the inherent increased linear stroke of oscillation. However, the transduction force generated by the piezoceramic disc(s) must increase with diaphragm area in order to achieve a given pressure amplitude.

#### **2. Mass Weighting**

"Mass weighting" is an attempt to force more oscillatory force from an individual piezoceramic disc. During operation, alternating current (AC) is fed to the disc(s), causing oscillation of the edges; in turn, each disc's center-of-mass attempts to remain stationary, causing the disc-center to oscillate 180° out-of-phase with respect to the edges. The pushrod and disc are connected at the disc-center, so the pushrod oscillates, causing diaphragm displacement. "Mass weighting" is accomplished by attaching small weights in a symmetrical pattern about the edge of the disc. See Fig. 6.1. As more mass is now oscillating at the edges, the disc-center must oscillate at a greater amplitude than in the unweighted case to keep stationary the center-of-mass. Since the inertial mass near the edge is increased, the maximum force generated at the center may also be increased. The result is theorized to be greater acoustic pressure.



Figure 6.1. Mass-weighting of a two-disc driver.

### 3. Number of Discs

Quite simply, more is better. To drive oscillation of the diaphragm, a one-disc driver must by itself overcome the combined mass of the pushrod and diaphragm as well as deliver force and power to the acoustic resistance of the resonator. It is theorized multiple discs will offer improved performance because the net load impedance is shared between the disks. In other words, this scheme is a force multiplier. It is important that during construction of a multiple-disc driver, the discs used all have nearly the same resonant frequency. This matching of discs helps to overcome any interference effects that could be dominant if the discs were all of a very different resonant frequencies.

### 4. Diaphragm Pre-flexing

Basically, the diaphragm is constructed by anchoring a very thin stainless-steel flat plate to the aluminum front plate. In its simplest form, the flexible stainless-steel plate is bonded to the rigid aluminum plate in a flattened state. The acoustically-driven flexing of the diaphragm is linear as long as the diaphragm's restoring force is predominantly flexural in nature and the tension is minimal. However, diaphragm displacements in the range of 50  $\mu\text{m}$  cause large internal tensions to be generated, limiting the maximum stroke in a nonlinear fashion.



Pre-flexing involves anchoring the diaphragm to the plate in an already displaced and slightly curved configuration. The comparison to use is instead of a rope being attached while taut, pre-flexing is the rope being attached with some slack.

## **B. PAST WORK**

For his thesis, LTJG Seyhmus Direk (Turkish Navy) did complete testing of drivers designated SN-01 and SN-02, and some preliminary testing of SN-03 – testing of SN-03 was completed as the first part of work for this thesis. What follows is a synopsis of the attributes of SN-01 and SN-02, as well as Direk's findings for each (for more information, see Direk, 2000). Direk's work with SN-03 is covered in the next chapter.

### **1. SN-01**

SN-01 is a 1-disc unweighted driver, with a certain diaphragm size. Direk found the optimum resonant frequency to be 4.30 kHz; testing the driver on the Test resonator ( $p_m = 150$  psia) at this frequency with driving voltage 14  $V_{rms}$ , a peak acoustic pressure differential of  $p_o = 3.63$  psi was found. This leads to a dynamic mean to pressure ratio of:

$$\frac{p_o}{p_m} = \frac{3.63}{150} = 2.42\%$$

Direk then went further, and in assuming SN-01 would produce the same  $p_o$  when  $p_m = 225$  psia, found the dynamic to mean pressure ratio to be:

$$\frac{p_o}{p_m} = \frac{3.63}{225} = 1.61\%$$

This ratio is well below the  $\frac{p_o}{p_m} = 5\%$  required for refrigeration. Direk concluded SN-01 qualitatively performed as expected, but just did not produce enough acoustic power.

### **2. SN-02**

SN-02 is a 2-disc unweighted driver, with a diaphragm size 21% larger than in SN-01. Direk reports SN-02's performance to be problem-ridden and below expectations – when not dealing with breakages between discs/electrical lead connections and

discs/pushrod joints, the driver delivered measurements 2.6 times lower than SN-01. This result led to a re-examination of data collected for SN-01.

In re-examining the data, a relationship was found between the mean pressure and its effect on peak acoustic pressure, diaphragm displacement, and volume velocity. As mean pressure increased:

- a. peak pressure increased,
- b. diaphragm displacement decreased, and
- c. volume velocity decreased.

It was therefore concluded the larger diaphragm of SN-02 had actually hindered performance – as a result, each following driver has been built with the same diaphragm area as SN-01. Another result is emphasis of research focusing upon the different disc arrangements and their effect on peak acoustic power.

## VII. MEASUREMENTS

### A. DRIVER SN-03

Driver SN-03 is a double-disc, unweighted driver with the same diaphragm size as SN-01. As part of his thesis, Direk was able to do enough testing on SN-03 to conclude it produced the acoustic power needed to produce some significant refrigeration. With this conclusion, construction of the Refrigerating resonator was accelerated so the first refrigeration tests could be conducted with SN-03.

The first task of this thesis was to find the resonant frequency of SN-03, using the Test resonator. The resonant frequency  $f$  of the driver was found to be  $f = 4.07$  kHz.

#### 1. Gas Resonance

An important premise of the MiniTAR's design is that the mechanical performance of the driver and the gas acoustics of the resonator both have moderately sharp resonances, and these resonant frequencies must be closely matched for efficient operation and high cooling power. Once constructed, the mechanical resonant frequency of the driver cannot be easily adjusted. While it is attempted to match the two resonant frequencies via the hardware design of the resonator, this is (generally) not precise enough to ensure success. However, the two resonances can still be matched, by introducing gas mixtures with different sound speeds.

The MiniTAR is designed to operate optimally with helium-krypton gas at 15 bar, but due to the gas's high cost, mixtures of helium and argon are used for testing. Before refrigeration measurements could be taken, the proper mix of helium and argon had to be found, the correct mix having the same resonant frequency as the driver.

To find the proper mix, the resonant frequencies of three different gases were measured. The Refrigerating resonator / SN-03 assembly was individually pressurized to approximately 10 bar with each of the following gases: pure helium (He), pure argon (Ar), and an argon-helium mixture consisting of 18% atomic argon (18% Ar-He). This latter mixture was available to us in a pre-mixed pressurized gas cylinder. The signal analyzer was then operated to make sweeps over a given frequency range at different drive voltages, producing curves like those plotted in Fig. 7.1.

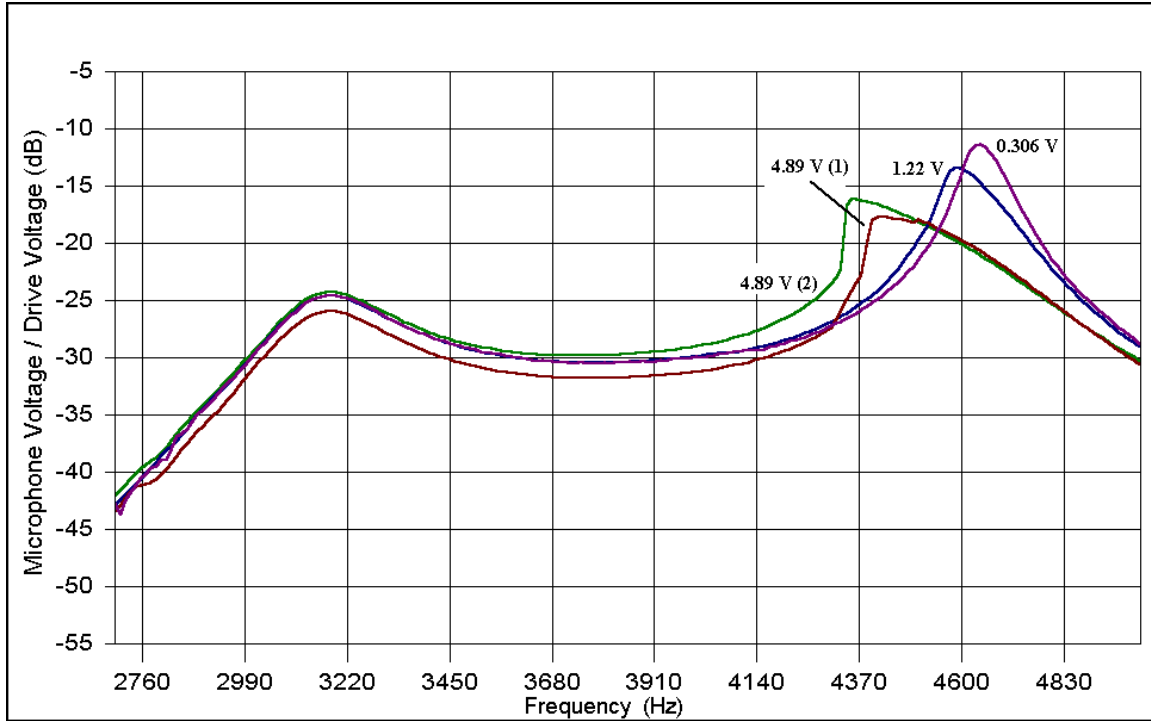


Figure 7.1. Resonance plot of 18% Ar-He. The peaks at 3.17 kHz denote the gas resonance, while the peaks on the right show the driver resonance.

Fig.7.1 shows a qualitative example of the results for each individual gas – the peak at  $f = 3.17$  Hz is the gas resonance, while the peaks in the interval  $f = (4.3, 4.8)$  kHz represent the driver resonances at different drive voltages. Note the driver resonance moves to the left as drive voltage is increased; the plot of "4.89 V (1)" is the acoustic amplitude after the first sweep with drive voltage  $4.89 \text{ V}_{\text{rms}}$ , while "4.89 V (2)" is the acoustic amplitude after three sweeps.

Fig. 7.2 is a combined plot of the resonances of the three individual gases. For the best refrigeration results, the gas resonance inside the Refrigerating resonator should be  $f = 4.07$  kHz, to match SN-03's resonance. As can be deduced from visual inspection of Fig. 7.2, none of the individual gases has the required resonance. The figure also shows that adding pure He to the 18% Ar-He mixture will produce the needed mixture. At this point, it would be simple to calculate the correct ratio of argon to helium, but unfortunately, the gas panel we used does not have the capability to mix gasses – therefore, a balancing act was performed in attaining the proper mixture.

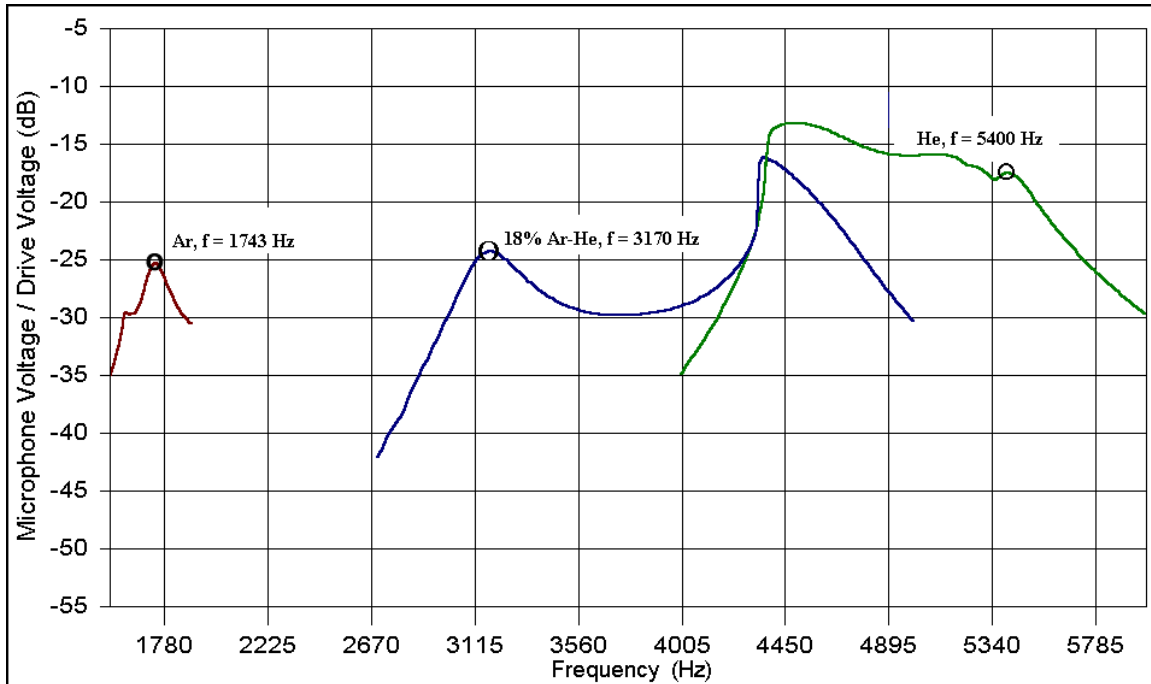


Figure 7.2. Individual gas resonances. The plots are not continuous over the entire range of frequencies as the frequency sweeps of interest were not in the same range.

The correct mix was found by first purging the system, then pressurizing to 10 bar with pure helium. At this point, the gas sound speed had to be "slowed-down", so the system was vented to approximately 5.5 bar, and repressurized back to 10 bar using the 18% Ar-He. The driver was then driven at  $0.722 V_{rms}$ , and the gas resonance viewed on the signal analyzer's screen – if the resonance was not 4.07 kHz, venting and repressurization was repeated. During the repetition, if resonance was above 4.07 kHz, 18% Ar-He was added, while if resonance was below 4.07 kHz, pure helium was added.

## 2. Refrigeration Tests

Temperature measurements were made using two thermocouples – one attached to the hot heat exchanger, and the other to the cold heat exchanger. See Fig. 7.3 for the location of the hot thermocouple.

The first refrigeration measurements were made at a room temperature of  $T = 23.8\text{ }^{\circ}\text{C}$ , with the Refrigerating resonator uninsulated and exposed to room conditions. Gas resonance was  $f = 4.10\text{ kHz}$ , and the assembly was driven at different frequencies (drive voltage  $14.0 V_{rms}$ ) to compensate gas resonance was not at the desired value. The

greatest temperature difference observed was 12.1 K, between  $T_C = 17.2\text{ }^{\circ}\text{C}$  and  $T_H = 29.3\text{ }^{\circ}\text{C}$ , at  $f = 4.03\text{ kHz}$ . The coldest  $T_C$  measured was  $T_C = 16.8\text{ }^{\circ}\text{C}$ .

The next set of measurements involved simulating a heat load on the refrigerator. An electric resistor (49.9  $\Omega$  metal film resistor rated at 0.25 W) was attached to the cold heat exchanger, and the entire assembly was insulated with polyester fiber-fill and a silvered Mylar<sup>TM</sup> outer covering. See Fig. 7.3 for location of the resistor. In preparatory testing, the resistor was run at different power settings (on a non-operating Refrigerating resonator) to ascertain the thermal impedance of the insulated resonator to the ambient. The data is shown in Table 7.1, and will be discussed in the next chapter.



Figure 7.3. Location of the thermocouple on the cold heat exchanger with the leads at top-right, and the resistor on the cold heat exchanger with leads at top-left.

<b>Heat Leak Measurement (1)</b>				
<i>Est P (W)</i>	<i>V (V)</i>	<i>I (mA)</i>	<i>hot T (°C)</i>	<i>cold T (°C)</i>
0.25	3.45	67.6	27.6	22.0
0.50	4.92	96.0	32.8	22.6
0.75	6.01	118	39.8	24.1

Table 7.1. Heat Leak Measurement Data.

After the thermal impedance was found, the system was purged and reloaded with the gas mixture that had resonance of 4.07 kHz. The first batch of measurements involved the assembly pressurized to 10 bar, driver operating at  $f = 4.07$  kHz. The second batch of measurements had the assembly pressurized to 13.4 bar and the driver operating at  $f = 4.02$  kHz. In both cases, drive voltage was  $V = 13.97 V_{\text{rms}}$  (i.e., full power). The variable for these tests was the resistor power; the resistor was operated at a certain power, and the recording of all data was taken once the temperatures of the hot and cold heat exchangers had stabilized. The resistor power was then changed, and the next recording of measurements were taken. The data taken is shown in Table 7.2, and with the thermal impedance calculations, will be analyzed in the next chapter.

<b>Refrigeration w/ Heat Load</b>			
<i>P (psia)</i>	<i>Resistor V (V)</i>	<i>hot T (°C)</i>	<i>cold T (°C)</i>
162.6	3.01	25.8	14.9
162.6	3.01	25.2	15.9
162.6	4.00	25.5	18.0
162.6	5.00	25.2	19.9
191.3	--	25.4	13.0
191.3	4.00	25.6	16.8
191.3	5.00	25.6	19.3

Table 7.2. Temperatures vs. Heat Load.

## B. SN-04

SN-04 is a two-disc weighted driver, with the same diaphragm size as SN-01 and SN-03. As always, the first benchmark was determining if the driver produced enough acoustic power for refrigeration.

To determine if SN-04 produced enough acoustic power, the data needed was the amplitude of the resonance peak at different pressures. To gather this data, SN-04 and

the Test resonator were pressurized to different pressures; at each pressure, the driver was run at full drive voltage ( $V = 13.8 V_{rms}$ ), and the plunger was adjusted until the frequency sweep on the signal analyzer showed only one resonance peak on a smooth curve. The data and analysis is shown in Table 7.3.

<b>SN-04 Power</b>			
<u><math>p_m</math> (psia)</u>	<u><math>A</math> (dB)</u>	<u><math>p_o</math> (psi)</u>	<u><math>p_o / p_m</math> (%)</u>
6.6	-65.2	0.0531	0.804
15.0	-56.4	0.146	0.975
26.0	-49.8	0.313	1.20
59.1	-41.4	0.822	1.39
101.5	-35.6	1.60	1.58
161.4	-29.5	3.24	2.00
225.7	-26.6	4.52	2.00

Table 7.3. Resonance peaks for SN-04 at different pressures.

In Table 7.3,  $p_m$  is the mean pressure, i.e. the pressure of the Test resonator / SN-04 assembly at which the data point was taken. The second column, "A", denotes the amplitude of the resonance peak, in decibels. The column  $p_o$  denotes the peak change in pressure due to the acoustic wave. The last column is the ratio  $\frac{p_o}{p_m}$ , denoted as a percentage.

The peak acoustic pressure  $p_o$  is found by converting the resonance peak to units of voltage, and then using the microphone's pressure-sensitive DC rating to convert the voltage to units psi. The equation used is:

$$p_o = (Drive\ voltage) * \sqrt{2} * 10^{\frac{A}{20}} * (PreAmp\ Gain)^{-1} * (Microphone\ sensitivity)^{-1}$$

$$p_o = 13.8(1000)\sqrt{2}\left(10^{\frac{A}{20}}\right)\left(\frac{1}{10}\right)\left(\frac{1}{20.22}\right) = 96.6\left(10^{\frac{A}{20}}\right)$$

The factor 13.8 is the rms drive voltage (which is used as the reference voltage for the dB in Table 7.3), and 1000 the conversion factor of volts to millivolts. The resonance peak amplitude is converted from decibels, and multiplied by  $\sqrt{2}$  to change from an rms value to a peak value. The scalar value of the amplitude, multiplied by the drive voltage, gives



the number of millivolts read at the signal analyzer. The result is further divided by 10 to offset the pre-amplifier's gain of 10, resulting in the number of millivolts actually sent by the microphone. The microphone has a sensitivity of sending  $20.22 \text{ mV}/\Delta\text{psi}$  -- the conversion then gives  $p_o$  in units psi-peak.

As can be seen from Table 7.3, the ratio  $\frac{P_o}{P_m}$  for SN-04 does not come close to the desired level of 5% for substantial refrigeration. Nor is it as powerful as SN-03, which demonstrated a  $\frac{P_o}{P_m}$  ratio of 2.9% in the test resonator.

### C. SN-05

SN-05 is a three-disc driver, with the same diaphragm size as SN-01, SN-03, and SN-04. Additionally, its microphone sensitivity is  $27.21 \text{ mV}/\Delta\text{psi}$ .

Unfortunately, during the driver's first run at full power, which corresponds to a drive voltage of  $13.8 \text{ V}_{\text{rms}}$ , the epoxy joint between one of the discs and the aluminum pushrod failed. Due to various budgetary and time constraints, the driver could not be repaired in time for further data to be collected for this thesis.

Data collected up to the time of breakdown, however, indicates SN-05 was performing admirably well. At a mean gas pressure of 154.8 psia and running at drive voltage  $13.8 \text{ V}_{\text{rms}}$ , the last recorded resonance peak was  $-19.6 \text{ dB}$ , indicating a

$\frac{P_o}{P_m} = 4.75\%$ . It should be noted this was the last known value only – the Test resonator

was not yet properly tuned when the breakdown occurred. Prior experience indicates the driver's resonant frequency is in the neighborhood of 4.1 kHz, and there is a good chance

that once repaired, SN-05 will meet and exceed the required  $\frac{P_o}{P_m}$  value.

THIS PAGE INTENTIONALLY LEFT BLANK

## VIII. ANALYSIS OF REFRIGERATION DATA

Analysis of the MiniTAR's refrigeration characteristics is best done by analyzing its performance when under heat load. As such, this chapter will first find the thermal impedance of the cold heat exchanger, i.e. the effects of the operating resistor, and will then use that result to compare the MiniTAR's performance to theory.

### A. THERMAL IMPEDANCE

The first part of Table 8.1 below simply restates the data of Table 7.1. For this data, the MiniTAR was not operating – all temperature changes are strictly the effect of heat dissipated from the resistor and thermal impedances in the structure and insulation.

<b>Thermal Impedance</b>							
<i>Est P (W)</i>	<i>V (V)</i>	<i>I (mA)</i>	<i>hot T (°C)</i>	<i>cold T (°C)</i>	<i>Heat (W)</i>	<i>DT (K)</i>	<i>Impedance (K/W)</i>
0.25	3.45	67.6	27.6	22	0.2280	5.6	24.56
0.50	4.92	96	32.8	22.6	0.4599	10.2	22.18
0.75	6.01	118	39.8	24.1	0.6948	15.7	22.60

Table 8.1. Determining thermal impedance.

The column "Heat" denotes the heat power of the resistor, calculated using the relation  $P = I^2 R$ , while  $\Delta T$  is simply the difference between the two heat exchanger temperatures. The thermal impedance is found through dividing the temperature difference by the input heat.

For the rest of our calculations, we will consider the thermal impedance to equal  $22.6 \pm 0.4$  K/W, i.e. the thermal impedance calculated when input heat power was 0.6948 W. Since the error of the temperature difference measurement dominates the net error, we chose the above thermal impedance value as the most accurate.

### B. REFRIGERATOR UNDER LOAD

While measuring the performance of the MiniTAR under heat load, the refrigerator was run at two different pressures: 10.0 bar and 13.4 bar. As the MiniTAR

was designed to operate at a pressure of 15 bar, only the data taken at  $p_m = 13.4$  bar is worthwhile to analyze.

Table 8.2 shows the total heat load on the refrigerator.

<b>Heat Leak Measurement (2)</b>						
<i>HeaterV (V)</i>	<i>T<sub>H</sub> (°C)</i>	<i>T<sub>C</sub> (°C)</i>	<i>HeaterP (W)</i>	<i>DT (K)</i>	<i>HeatLeak (W)</i>	<i>HeatLoad (W)</i>
0.00	25.4	13.0	0.000	12.4	0.549	0.549
4.00	25.6	16.8	0.308	8.8	0.389	0.697
5.00	25.6	19.3	0.481	6.3	0.279	0.760

Table 8.2. Determining total heat load on the MiniTAR.

For measured values, the column "HeaterV" shows the measured voltage across the resistor, and columns "T<sub>H</sub>" and "T<sub>C</sub>" denote the temperatures at the hot and cold heat exchangers, respectively. "HeaterP" is the heat load from the resistor itself, the power calculated as  $P = V^2/R = V^2/52$ . The resistance for this equation is 52  $\Omega$  instead of the resistor's  $R = 49.9 \Omega$  to offset any heat leak caused by heating of the copper wires used to connect the resistor to the DC power supply; though very small-gauge wires were used, in order to minimize the heat leak, we feel this is a prudent step. The "Heat Leak" is the temperature difference between heat exchangers divided by the thermal impedance; this measures how much additional heat load the MiniTAR puts on itself simply because it is sustaining a temperature difference. The total heat load is the sum of the resistor's power and the heat leak.

The above analysis makes possible some interesting comparisons, among them the "hot temperature" when the MiniTAR was off and subject only to the resistor's heating, to the "hot temperature" when the MiniTAR was on and operating with an equivalent heat load. When the MiniTAR was off and the resistor was producing approximately 0.7 W of power, the hot temperature approached 40 °C. When the MiniTAR was on and had a heat load of 0.76 W, the hot temperature stabilized at 25.6 °C – proving that the MiniTAR is, indeed, refrigerating.

Another comparison involves comparing values when  $\Delta T$  is similar. For this, consider when the MiniTAR was off, and the resistor was producing  $P = 0.4599$  Watts –

the resulting  $\Delta T$  was 10.2 K (cold temperature was 22.6 °C). The most similar  $\Delta T$  produced during refrigeration is 8.8 K (hot temperature was 25.6 °C), produced under a heat load of 0.697 W. Consider: the resistor, operating at a certain power, itself causes a certain temperature differential. The MiniTAR, when operating with a slightly-higher heat load, produces a slightly-lower temperature differential – with its "hot" temperature just 3 K above the "cold" temperature when only the resistor was operating. Taken all together, these arguments indicate the MiniTAR is producing about 0.5 W of refrigerating power.

A better analysis can be done when comparing actual figures-of-merit to theoretical, as done in Table 8.3. All of the theoretical quantities were calculated in DSTAR, using the MiniTAR model.

<b>Actual vs. Theoretical</b>						
<i>HeaterV (V)</i>	<i>Mic (mV)</i>	<i>po/pm (%-pk)</i>	<i>DrivePT(W)</i>	<i>COPT</i>	<i>COPM</i>	<i>COPDiff(%)</i>
0.00	886	2.44	0.340	2.33	1.61	-30.8
4.00	862	2.38	0.339	2.48	2.06	-17.2
5.00	852	2.35	0.340	2.58	2.24	-13.1

Table 8.3. Actual Figures-of-Merit vs. Theoretical.

The "HeaterV" column denotes the data, and measured values, correspond to the same data points of Table 8.2. The microphone (mic) data leads to finding the ratio  $\frac{P_o}{P_m}$  -- note

that though SN-03 produced  $\frac{P_o}{P_m} = 2.9 \%$  with the Test resonator, performance is

degraded when paired with the Refrigerating resonator.

The column "DrivePT" is a mixed measured and theoretical value; the combination of the measured  $(p_o/p_m)^2$  divided by the theoretical acoustic impedance, it reflects how much acoustic power is produced at the driver diaphragm. While in the past we have acquired direct acceleration measurements of the driver piston for the purpose of direct acoustic power measurement, the extremely small size of the driver components made it impossible to use this technique. Hence, we resorted to a mixed measurement and theory estimate of acoustic power.

The measured-COP (COPM) is a combination of theory and measurement; it is the quotient of the corresponding heat load divided by the (theoretical) Drive Power ("DrivePT"). The listed COPT values are purely theoretical determinations computed through DSTAR.

Note, all COP's listed incorporate the thermal conduction heat leak as part of the net heat load on the refrigerator. While this does not properly reflect the usable refrigerator performance, as would be required for the sale of a commercial product, it does simplify the comparison between experiment and theory.

## **IX. CONCLUSIONS**

### **A. DRIVER-POWER IMPROVEMENT SCHEMES**

Four different ideas were proposed to improve driver power: larger diaphragm area, mass weighting, number of piezoceramic discs, and diaphragm pre-flexing. A previous thesis (Direk, 2001) concluded larger diaphragm area had an adverse effect on driver performance. As a result, all drivers constructed since have had a diaphragm area equal to SN-01.

Driver SN-03 is a two-disc, unweighted driver, and SN-04 a two-disc, weighted driver. The fact that SN-03 was used for the first refrigeration tests, and SN-04 was proven to not possess enough acoustic power for refrigeration, suggests that mass weighting adversely affects driver performance. Proving the ineffectiveness of mass weighting would require building and testing a small ensemble of weighted drivers, which is too time consuming for our project. It is always possible that poor performance of a single unit results from one or more errors in fabrication.

The last driver tested for this thesis, SN-05, is a three-disc unweighted driver with a pre-flexed diaphragm. Unfortunately, the epoxy joint between the aluminum pushrod and one of the piezoceramic discs failed during testing, and repairs could not be completed in time for this thesis. Although no conclusions can be drawn upon the effects of diaphragm pre-flexing and increasing the number of piezoceramic discs, initial signs point toward the combination ultimately improving driver power. Further testing is encouraged.

### **B. MINI-TAR REFRIGERATION**

The initial refrigeration tests, making use of driver SN-03, were intended to analyze how closely the measured thermoacoustic values of the constructed unit compared to theory. At worst, the MiniTAR performed 30.8 % below theorized values; at best, performance was 13.1 % below expected.

The main problem of this project is its scale – the MiniTAR is the first attempt to build a thermoacoustic refrigerator that is two inches tall and can produce 0.5 W of

cooling power when creating a  $\Delta T = 30$  K. The MiniTAR coming within 13.1 % of expected performance (at best) signifies continued research is worthwhile. Of note is the MiniTAR was designed to operate with a peak  $\frac{P_o}{P_m}$  ratio of 5 %; during the testing, the peak  $\frac{P_o}{P_m}$  ratio did not exceed 2.5 %. Therefore, the acoustic driver power was too low by a factor of four. More work is needed to increase driver power.

### C. RECOMMENDATIONS OF FUTURE WORK

Driver SN-05 should be repaired, and testing fully completed, to draw a clear conclusion of how driver power is affected by diaphragm pre-flexing and more (i.e., three) piezoceramic discs. If possible, an additional driver should be constructed; this new driver (SN-06) should either be a two-disc unweighted driver with a pre-flexed diaphragm, or a three-disc unweighted driver with the same diaphragm as SN-01. Testing of the proposed SN-06 would isolate the effects of three discs or the pre-flexed diaphragm.

The epoxy failure on SN-05 is a failure similar to what was experienced with SN-02. The epoxy failure on both drivers points to the need for more research on alternate driver designs, ones in which critical joints are not simply glued together. Unfortunately, the small scale of the project will make alternate driver designs difficult. This design challenge will probably hamper future MiniTAR development.

### D. OVERALL

Thermoacoustics is an exciting world, a field in which refrigeration can be obtained without the use of any chemicals. Thermoacoustic theory is well-established; its main drawback is the myriad of engineering challenges to make it work, especially on a scale as small as the MiniTAR.



## **LIST OF REFERENCES**

Berhow, T.J., "Construction and Performance Measurement of a Portable Thermoacoustic Refrigerator Demonstration Apparatus", December 1994.

Brookes, B.R., "Construction of a Thermoacoustic Refrigerator Demonstration Apparatus", March 1994.

Direk, S., "Design of a Mini Thermo-Acoustic Refrigerator", March 2001.

Livvarcin, O., "Design and Cost-Benefit Analysis of a Mini Thermo-Acoustic Refrigerator Driver", September 2000.

Purdy, E.W., "Development of a Graphical Numerical Simulation for Thermoacoustic Research", December 1998.

Swift, G.W., "Thermoacoustic Engines", Journal of the Acoustical Society of America, v.84, pp. 1145-1179, 1988.

Swift, G.W., "Thermoacoustic Engines and Refrigerators", Physics Today, pp. 22-28, July 1995.

THIS PAGE INTENTIONALLY LEFT BLANK

## INITIAL DISTRIBUTION LIST

1. Defense Technical Information Center  
Ft. Belvoir, Virginia
2. Dudley Knox Library  
Naval Postgraduate School  
Monterey, California
3. Thomas J. Hofler, Code PH/HF  
Naval Postgraduate School  
Monterey, California
4. Bruce Denardo, Code PH/DE  
Naval Postgraduate School  
Monterey, California
5. Jeffrey F. Denatale  
Rockwell Science Center  
Thousand Oaks, California
6. C. L. Chen  
Rockwell Science Center  
Thousand Oaks, California
7. Department of Physics  
Naval Postgraduate School  
Monterey, California